

Detection of single-mode thermal microwave photons using an underdamped Josephson junction

Received: 3 July 2024

Accepted: 8 January 2025

Published online: 11 April 2025

 Check for updatesA. L. Pankratov^{1,2} ✉, A. V. Gordeeva¹ ✉, A. V. Chiginev^{1,2}, L. S. Revin^{1,2},
A. V. Blagodatkin^{1,2}, N. Crescini^{3,4} & L. S. Kuzmin^{1,5,6}

When measuring electromagnetic radiation of frequency f , the most sensitive detector counts single quanta of energy hf . Single photon detectors have been demonstrated from γ -rays to infrared wavelengths, with ongoing efforts to extend their range to microwaves. Here we show that an underdamped Josephson junction can detect 14 GHz thermal photons, with energy 10 yJ or 50 μ eV, stochastically emitted by a microwave copper cavity at millikelvin temperatures. After characterizing the source and the detector, we vary the cavity temperature and measure the photon rate. The device achieves 45% efficiency and a dark count rate of 0.1 Hz over several GHz. Demonstrated super-Poissonian photon statistics is a signature of thermal light and a hallmark of quantum chaos. We discuss applications in dark matter axion searches and note its relevance to quantum information and fundamental physics.

Photons, the quanta of light, are massless particles whose energy E is related to their frequency f by Planck's constant h , through the relation $E = hf$ ¹. The most energetic photons ever recorded, with $E > 100$ TeV, belong to the class of gamma rays, which extend down to $E \sim$ MeV². Lower energy photons, such as X-rays, have energies around $E \sim$ keV^{3–5}. Single photons in the gamma and X-ray ranges are detected using high-energy physics techniques, such as crystal scintillators and photomultiplier tubes⁶. In the optical domain, where photons typically have energies of $E \sim$ eV, single-photon detection is well-established, utilizing devices like photomultipliers and avalanche photodiodes⁷. Advancements in superconducting technologies have enabled photon detection in the infrared range ($E \sim$ meV), employing methods such as nanowires^{8,9}, transition-edge sensors¹⁰, kinetic inductance detectors⁵, and Josephson junctions⁴.

The microwave range, with photon energies around $E \sim 50 \mu$ eV (~ 10 yJ), represents the frontier of single-photon detection¹¹. This range has been explored using quantum dots¹² and bolometric schemes^{13–15}. The development of single-photon detectors (SPDs) in the microwave range has drawn significant interest from the field of

quantum technologies. Circuit quantum electrodynamics schemes¹⁶ have been proposed^{17,18} and implemented with qubits^{19–26}.

The demand for microwave SPDs is exemplified in dark matter searches, such as those for axions^{27–29}. In particular, dark matter haloscopes^{30–33} rely on precision power measurements using low-noise amplifiers. Transitioning to photon detectors is crucial^{34,35} as they outperform quantum-limited amplifiers and quantum-enhanced measurement techniques, especially at higher frequencies (above a few GHz) where the standard quantum limit of linear amplification significantly hinders sensitivity^{34,36}.

The axion signal, characterized by a stochastic emission of rare photons at frequency f_a , depends on the unknown axion mass and has a narrow bandwidth of $10^{-6}f_a$ ²⁷. Consequently, suitable photon detectors must exhibit a low dark count rate, wide spectral range, high efficiency, and continuous operation capabilities. Existing microwave photon detectors generally fall short of these requirements, although some recent experiments^{24,37} have addressed these challenges. Josephson junctions have been proposed and analyzed as threshold detectors for microwave photons^{38–44}. While they have been realized

¹Nizhny Novgorod State Technical University n.a. R. E. Alekseev, Nizhny Novgorod 603950, Russia. ²Institute for Physics of Microstructures of RAS, Nizhny Novgorod 603950, Russia. ³Fondazione Bruno Kessler (FBK), I-38123 Trento, Italy. ⁴Univ. Grenoble Alpes, CNRS, Grenoble INP, Institut Néel, 38000 Grenoble, France. ⁵Chalmers University of Technology, 41296 Gothenburg, Sweden. ⁶Deceased: L. S. Kuzmin. ✉e-mail: alp@ipmras.ru; a.gordeeva@nntu.ru

for detecting high photon rates⁴⁴, their use in detecting rare photons remains an experimental challenge.

In this work, we demonstrate the detection of single microwave photons with high efficiency and a sub-hertz dark count rate using an underdamped Josephson junction (JJ). The photons are generated via thermal emission from a bulk copper resonator. The experimental scheme and operation principles are illustrated in Fig. 1. The cavity design determines the frequency of the emitted photons, and the emission rate is adjusted from less than one photon per hour to thousands of photons per second by varying the cavity temperature. The photons are collected by the detector using an on-chip impedance-matching line terminated by a JJ. When a photon impinges on the detector, the current-biased JJ switches to the resistive state, producing a detection event. The observed thermal photons depend exponentially on temperature and, when sourced from a single mode, follow a super-Poissonian statistics^{45,46}, providing a unique signature of their nature⁴⁷.

Results

Experiment concept

The experiment consists of two main components: a photon source and a photon detector, as shown in Fig. 2. The photon source is a cylindrical cavity with a radius of 3.0 cm and a height of 1.2 cm (Fig. 2a). The cavity body is made of oxygen-free, high-conductivity copper, ensuring effective thermalization and a quality factor of approximately 10^4 . The cavity is coupled to two SMA ports: port 1, weakly coupled, is used for characterization, while port 2 is close to critical coupling. The measured S_{21} transmission of the resonator, shown in Fig. 2b, reveals the first four resonant modes.

The detector is an underdamped Al-AlO_x-Al Josephson junction connected to the cavity antenna. When a photon is absorbed, the junction switches to the running state, producing a measurable voltage drop of hundreds of microvolts. Figure 2c shows the circuit diagram, chip layout, optical images, and an SEM image of the Josephson junction. The on-chip coplanar line is designed as an impedance transformer from 50 Ω to 200 Ω. Simulations indicate that the matching efficiency exceeds 60% even for junctions with R_N values up

to 2 kΩ. The detector's bandwidth is ~3 GHz around 14 GHz, with a subband near 8.8 GHz linked to internal resonances of the JJ sample.

Microwave signals from cavity port 2 are delivered through a short coaxial cable soldered to the PCB coplanar line, which is bonded to the chip's coplanar line. Bias and voltage line T-filters consist of feed-through capacitors (1.1 nF, red), on-plate resistors (500 Ω, blue), and external resistors (10 kΩ, not shown). The output voltage is read using a room-temperature AD745 amplifier and analog-to-digital converter.

The setup with the cavity mounted on the coldest plate of a dilution refrigerator is shown in Fig. 2d. The SPD is housed inside cryoperm and superconducting screens to minimize magnetic noise and stray light. A SQUID thermometer on the cavity ensures precise temperature control, while a 5 Ω heating resistor is installed at the cavity base. Measurements of the SPD's response to the resonator's signal were conducted by varying the heating temperature from 21 mK to 80 mK, corresponding to heating resistor voltages of 0 mV to 28 mV. The SPD's copper base is anchored directly to the mixing chamber plate to reduce heat transfer through the SMA connector. SPD switching time measurements were automated, enabling precise feedback for cavity and cryostat plate temperatures.

The SPD was fabricated using the shadow evaporation technique, forming an Al-AlO_x-Al trilayer on a Si substrate with an area of $2.5 \times 0.7 \mu\text{m}^2$, see Methods. At 17 mK, the measured critical current is $I_C = 170$ nA, and the normal state resistance is $R_N = 1480$ Ω (Fig. 3a). The chosen parameters balance reduced dark count rates and optimal quantum efficiency, targeting a regime that minimizes thermal activation and quantum tunneling events⁴². The critical current and damping allow operation in the phase diffusion regime^{44,48}, enhancing performance. The detector response time, determined by the inverse plasma frequency, is below 1 ns. The detector's dead time, governed by RC filters, is 2–10 ms. An example of a single-shot measurement with 3 ms bias current rise and fall times and a 42 ms switching time is shown in the inset of Fig. 3a.

Sequential measurements of the SPC-73 sample's current-voltage characteristics confirm setup stability (Fig. 3a). The critical current at 17 mK, $I_C = 170$ nA, approaches the Bardeen-Cooper-Schrieffer (BCS) theoretical limit of 197 nA in the absence of

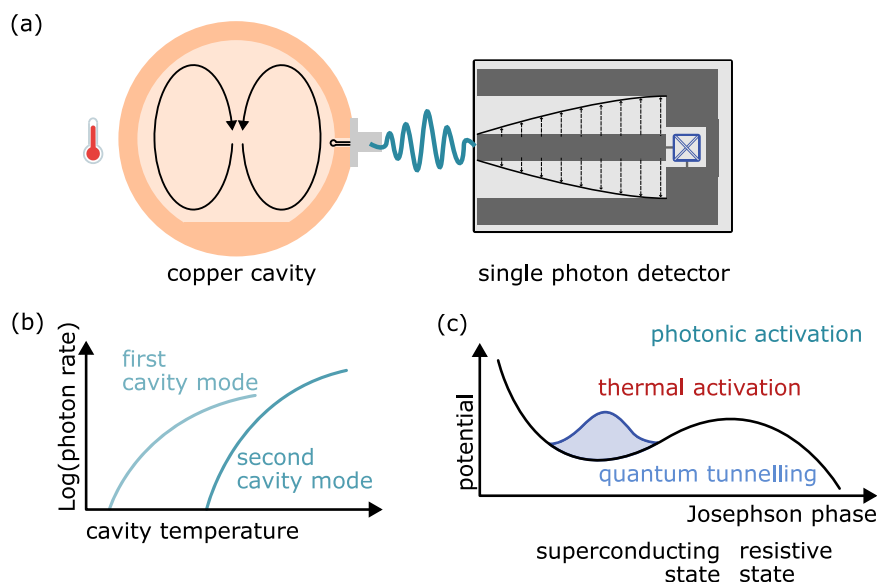


Fig. 1 | Description of the experimental scheme. **a** A microwave cavity is connected to the photon detector, where the former acts as a source of thermal photons and the latter is formed by the Josephson junction, inserted into a coplanar waveguide adapter. **b** Temperature dependence of the rate of thermal photons emitted by the cavity. With a corresponding temperature change of tens of millikelvin, the photon rate is varied by orders of magnitude. **c** The tilted washboard potential describes the dynamics of a Josephson junction: the system is superconducting if the wavefunction is confined to a minimum, and resistive if it runs down the potential. The switching to the resistive state can be due to the arrival of a photon, or due to noise, appearing as thermal escape or quantum tunnelling processes, which therefore needs to be suppressed.

potential describes the dynamics of a Josephson junction: the system is superconducting if the wavefunction is confined to a minimum, and resistive if it runs down the potential. The switching to the resistive state can be due to the arrival of a photon, or due to noise, appearing as thermal escape or quantum tunnelling processes, which therefore needs to be suppressed.

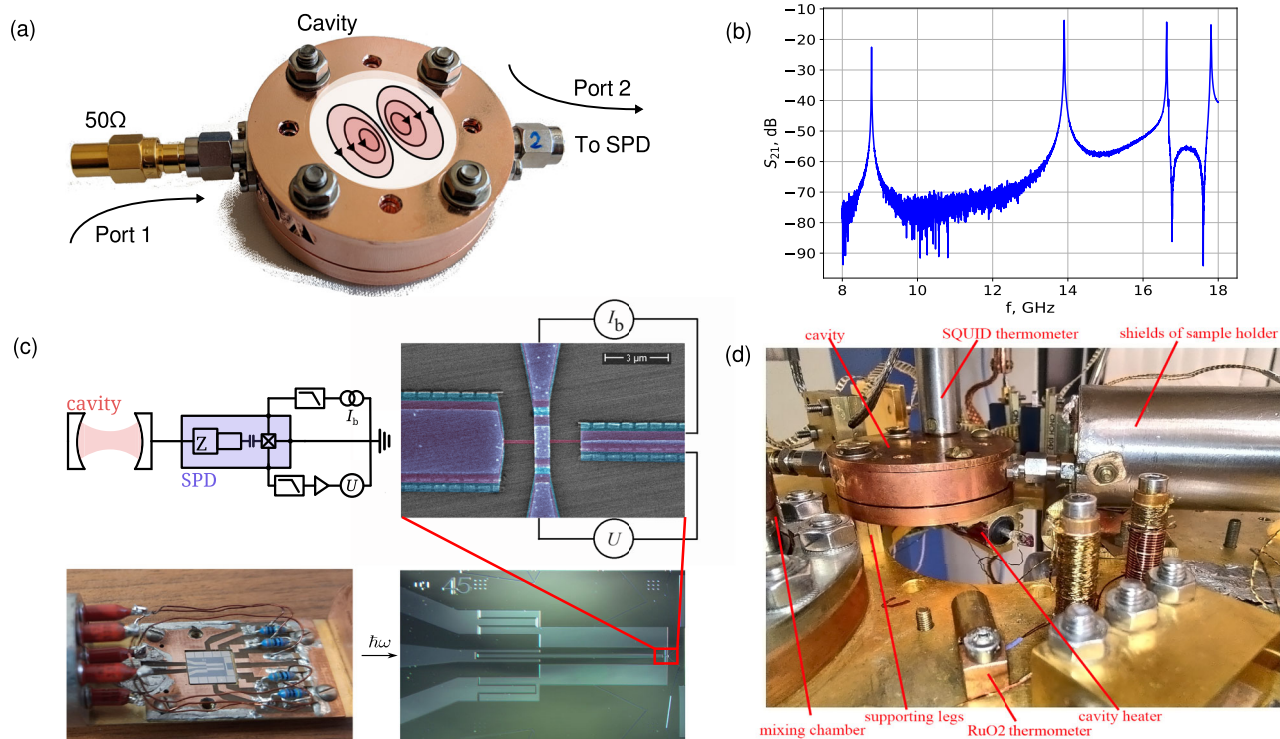


Fig. 2 | Microwave cavity and photon detector used in this work. **a** The cavity, critically coupled to the SPD through antenna port 2, while port 1 is weakly coupled and used for characterization purposes. At the center of the cavity, a sketch of the 14 GHz mode shape is shown. **b** Room-temperature response of the cavity, showing resonant modes starting from the fundamental mode at 8.81 GHz. A comparison with resonances at 17 mK is provided in Fig. 4. **c** Circuit diagram with optical images of the detector connected to the cavity antenna and mounted in the sample

holder. SEM image of the Josephson junction with artificial colors: pink - bottom Al electrode, blue - top Al electrode, violet - overlapping areas. The feeding dc lines are also shown, indicating the bias current I_b and measured voltage U . **d** Picture of the coldest plate of the dilution refrigerator, showing the sample holder within the cryoperm screen and the copper cavity. A SQUID thermometer is mounted on top, with a heating resistor installed below.

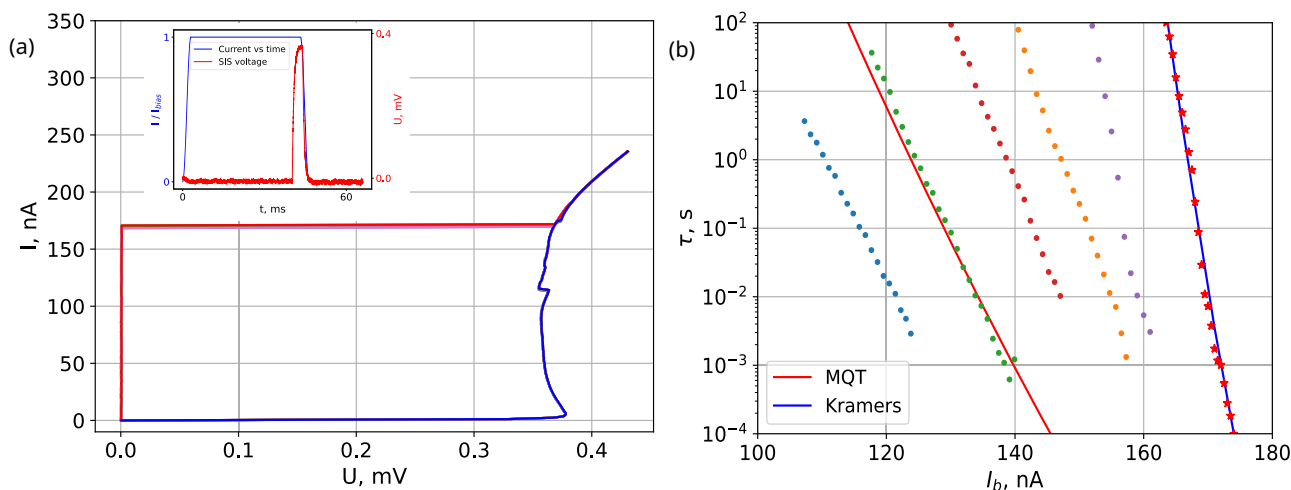


Fig. 3 | Preliminary characterization of the detector. **a** Current-voltage characteristics of the sample at 17 mK, sequentially measured 10 times to demonstrate setup stability. Inset: Example of a single-shot measurement with bias current rise and fall times of 3 ms each. **b** Mean switching times of the SPD at 17 mK, showing

significant reductions in dark counts due to filtering improvements over several months (dots - experiment, solid curves - theory). Error bars are smaller than the dot size.

thermal and quantum noise. Figure 3b shows the mean switching time of the SPC-73 sample, demonstrating significant reductions in dark counts through iterative filtering and screening improvements. Theoretical tunneling time predictions^{38,49,50} (red solid curve) match closely the experimental data after improvements. Stray light mitigation efforts yielded the rightmost curve (red

dots), surpassing the standard tunneling time limit. This points to the onset of the quantum phase diffusion regime⁴⁴, where the dark count rate decreases significantly. Interestingly, the rightmost data align with the classical Kramers' time predictions⁵¹, fitting at 18 mK a critical current value of 191 nA, consistent with the BCS theoretical limit for this sample.

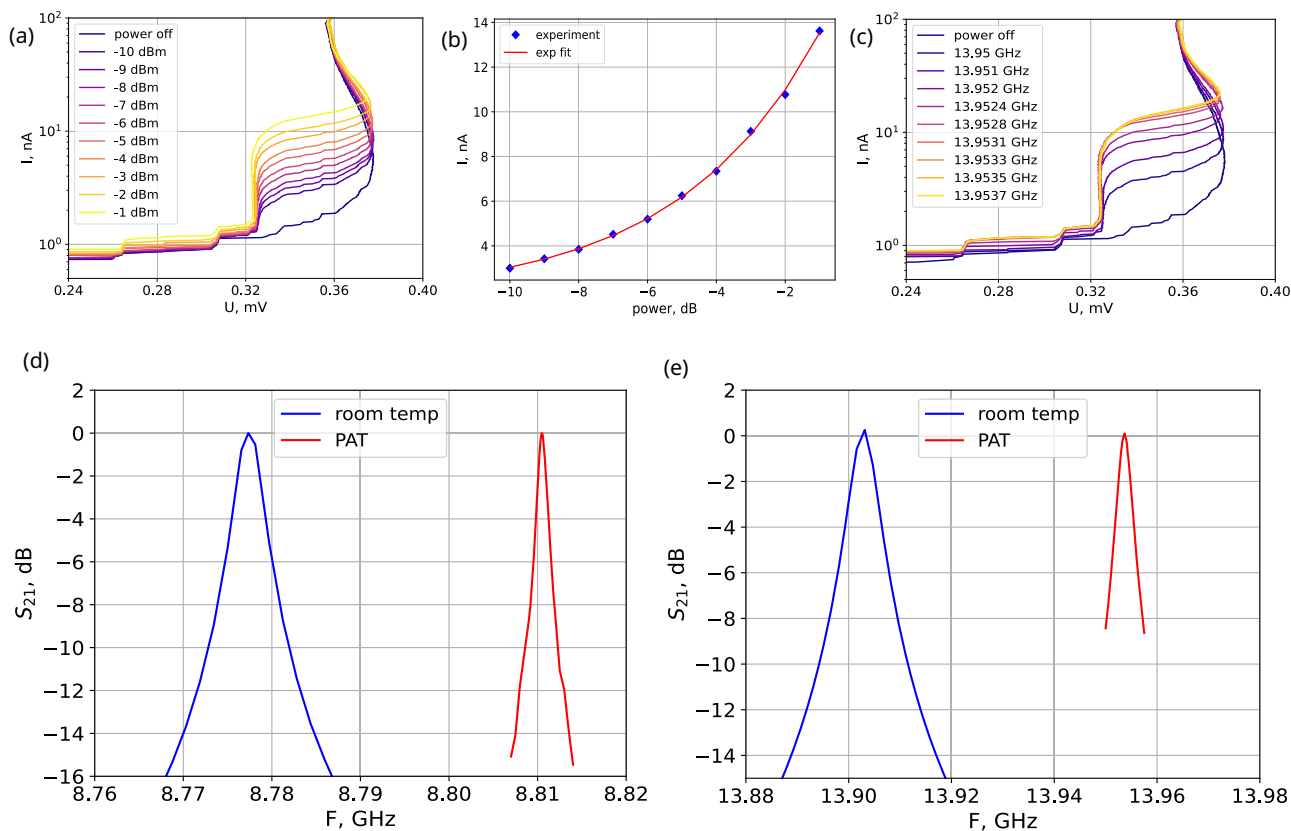


Fig. 4 | Measurements of cavity resonances by photon-assisted tunneling steps of the SPD. **a** IV curves at various incident radiation powers and constant frequency of 13.9537 GHz; **b** Calibration curve to translate the position of current step to dB; **c** IV curves at various frequencies of incoming radiation and constant power; **d, e** Comparison of frequency response of the cavity measured at room temperature by

VNA (blue) and at 17 mK measured by photon-assisted tunneling steps in SPD (red). **d** Resonance at 8.8 GHz, **e** resonance at 13.9 GHz. Both dependences are normalized to the same level so that their maxima are at 0 dB. Blue curves are actually the enlarged curves from Fig. 2b.

Measuring the cavity resonances

An underdamped Josephson tunnel junction is well-known as a detector of a harmonic signal with a minimum detectable power down to the femtowatt level, by measuring the photon-assisted tunneling (PAT) steps at the inverse branch of a current-voltage characteristic. In this work, we use PAT steps (see Methods) to measure resonant curves of the cavity at low temperatures.

To correctly fit the measured photon rate with the theory, see below, we must properly characterise the cavity quality factors as well as their central frequencies and substitute these values into Eq. (1). The resonator has four resonant frequencies: 8.81 GHz; 13.95 GHz; 16.67 GHz and 17.85 GHz, but the rate of photon emission at frequencies 16.67 GHz and 17.85 GHz is more than one order of magnitude lower than at the other two frequencies. Therefore, when determining the SPD efficiency, only modes at 8.81 GHz and 13.95 GHz were taken into account.

The method for measuring the cavity resonances with using the PAT steps is as follows. First of all we measure a series of IV curves at a frequency close to a resonance with various microwave power values (Fig. 4a). Then we plot the calibration curve that shows the dependence of the current step position on the supplied microwave power in dB at a certain voltage on the SPD (Fig. 4b, blue diamonds). We make an exponential fit of the calibration curve and thus have the dependence of the incident power on the current step position at any value between the measured points (Fig. 4b, red curve). Then, finally, we measure IV curves at a constant supplied microwave power with frequencies varying in the vicinity of the cavity resonance (Fig. 4c). Using the calibration curve obtained at the previous step we transform the

positions of the current step into the value of the incident power in dB. Since we make such measurements near the resonant frequency, the incident power strongly depends on the frequency of the microwave signal. The frequency response of the cavity near 8.8 GHz (d) and 13.9 GHz (e) measured by the PAT steps (red curves) are presented in Fig. 4d, e. For comparison, we plot the room temperature frequency response of the cavity, measured with a VNA (blue). We see that the quality factor at low temperature 17 mK increases, as expected, with a simultaneous shift of the resonant frequencies to slightly higher values. Thus, at low temperatures, the quality factor of the 8.81 GHz mode reaches $Q_1 = 7340$, and the one of the 13.9 GHz mode is $Q_2 = 4650$. The measured values of quality factors and central frequencies are used for fitting of the measured photon rate with the theory in Eq. (1), shown in Fig. 5.

Detecting single photons, thermally emitted from the cavity

The average number of thermal photons in a cavity mode follows the Planck distribution and depends on the modes' resonance frequency, loaded quality factor, and temperature. Dissipation regulates the photon lifetime, giving rise to an emission rate that can be controlled by coupling an antenna to the mode⁵². On first approximation, the cavity photon rate $r_c(T)$ measured with an SPD can be calculated considering n modes as

$$r_c(T) = \sum_{i=1}^n \frac{\eta_i}{\tau_i} \frac{1}{e^{hf_i/k_B T} - 1} \quad (1)$$

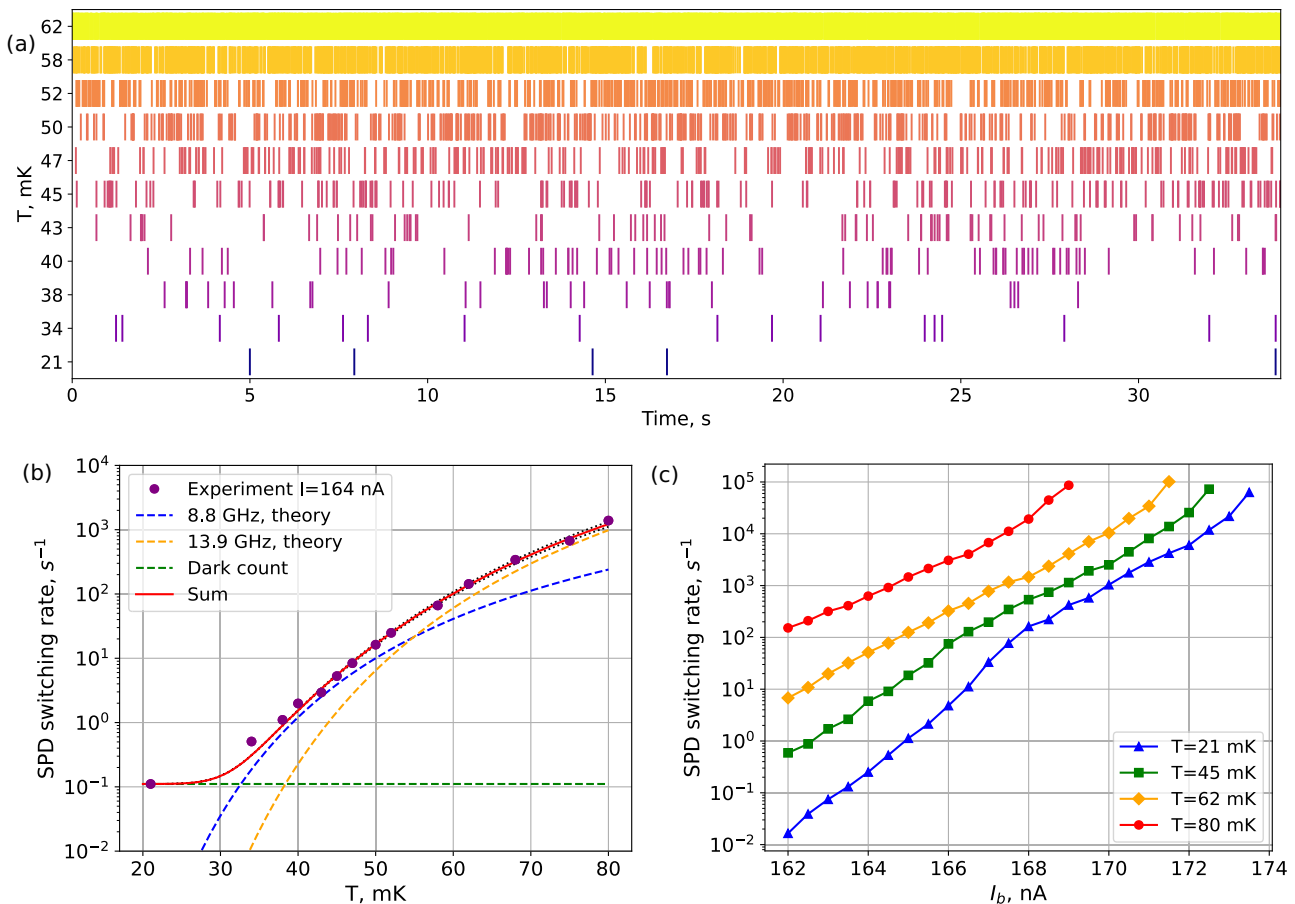


Fig. 5 | Single microwave photon detection. **a** An event plot of the recorded data is shown at various temperatures of the cavity. **b** The SPD switching rate, fitted with the theoretical photon rate, using formula (1). The error bars do not exceed the dot sizes due to 5000 averages. The data are fitted with the expected cavity photon rate r_c (1) (red solid curve) plus a dark count rate r_{DC} (green dashed line) to extract the

efficiency and noise floor of the detector. The black dotted curves show $\pm 0.05 \eta_2$ spread of the fitting. The values of quantum efficiency η reach 0.0125 and 0.45 ± 0.05 for 8.81 GHz and 13.9 GHz modes, respectively. **c** The SPD switching rates versus bias current, measured at the base temperature 17 mK, for various cavity temperatures from 21 to 80 mK.

where f_i , τ_i are the frequencies and the lifetimes of the cavity modes' photons, respectively; h is the Planck constant, k_B is the Boltzmann constant and T is the temperature. The photon lifetime $\tau_i = Q_i/(2\pi f_i)$ is extracted from the quality factor Q_i of the mode and its central frequency f_i . The parameter η_i is the ratio between the thermally available photons of the i -th cavity mode and the detected ones. It depends on the cavity antenna coupling and on the detector quantum efficiency. The fact that the antenna is critically coupled to the cavity means that only a half of available photons exit the cavity and go to the detector. Thanks to the exponential dependence of the rate on the $hf_i/k_B T$ ratio, at low enough temperatures only a limited number of modes significantly contribute to the rate, allowing us to neglect the effect of higher-order resonances.

To observe the variation of the photon rate and characterise the quantum efficiency and dark count rate of the detector, we measured the temperature dependence of the switching events. To this end, the temperature of the cold plate of a dilution fridge was fixed at about 17 mK, while the cavity, weakly thermally coupled to the plate, was heated by a resistor to a temperature of 21 to 80 mK, precisely controlled using a SQUID noise thermometer. An estimate of a photon-induced current pulse is given in Methods.

In Fig. 5a we present an event plot of the recorded data at various cavity temperatures, from 21 to 62 mK, showing an exponential increase of the switching rate. Figure 5b displays the switching rate versus temperature and its fit. We fit the data with the expected cavity photon rate $r_c(T)$ in Eq. (1) plus a dark count rate $r_{DC} = 1/\tau_0$, which is the

inverse of the mean switching time τ_0 taken from the lowest temperature data, to extract the efficiency and noise floor of the detector. For this analysis, the quality factors and resonance frequencies are fixed to the values measured using PAT steps, see Fig. 4. In particular, at $f_1 = 8.81$ GHz, $Q_1 \approx 7340$, and at $f_2 = 13.95$ GHz, $Q_2 \approx 4650$. Figure 5b shows a good agreement between the expected cavity photon rate and the experiment. From this data, we verify that only the first two modes contribute to the detector response at these temperatures, while the higher frequency modes are irrelevant. The detection efficiency η_2 is as high as $45 \pm 5\%$ for the mode f_2 , with a dark count rate of 0.1 Hz. In this experiment, the estimated efficiency is a convolution between the antenna coupling and the detector efficiency, and is therefore a lower limit. For instance, $\eta_1 \approx 1\%$ is mainly due to the weak coupling of the antenna to the mode f_1 , as can be deduced from Fig. 2b, as well as SPD coplanar antenna selectivity, aimed to efficiently receive 14 GHz photons. The choice of the antennas' couplings is tailored to swap the main contribution to $r_c(T)$ from f_1 to f_2 at a temperature of about 50 mK, therefore forming a peculiar cavity response, as shown in Fig. 5b.

In Fig. 5c, the SPD is characterised by measuring its mean switching rate versus bias current for various cavity temperatures. The mean switching rate coincides with the SPD dark count rate at the lowest cavity temperature of 21 mK in the absence of thermal photons, while it is defined by the photon rate at a large cavity temperature. One can see that the switching rate, starting from 0.01 Hz at the smallest bias current, increases by four orders of magnitude when heating cavity up to 80 mK, demonstrating the efficient response to incoming

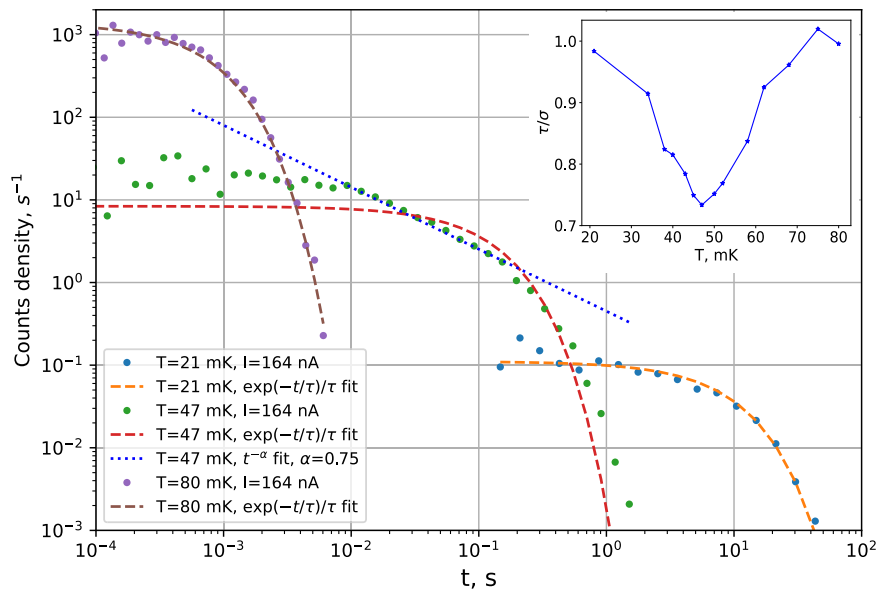


Fig. 6 | Distribution of times between sequential switchings of the SPD at three various temperatures. The experimental data (dots) are fitted by $\exp(-t/\tau)/\tau$ (dashed curves) without any fitting parameters with the mean switching time τ directly taken from experimental data. Good agreement between fitting and

experiment is observed at 21 mK and 80 mK cavity temperatures. One can note super-Poissonian distribution at intermediate cavity temperature 47 mK. Inset: The τ/σ ratio vs cavity temperature, showing deviation from Poissonian statistics.

photons. It was checked that the dark count rate nearly does not change at the same cavity temperature variation if the sample is disconnected from the cavity, and also that the response is heavily suppressed if the cavity is connected to the SPD by the port 1.

Since a signature of single-mode thermal photons is their super-Poissonian statistics⁴⁵, let us study the ratio of the SPD mean switching time τ to its standard deviation σ . It is known that in the case of Poissonian statistics, which is a natural statistics of thermal or quantum dark counts of our detector, this ratio should be equal to unity⁵¹. In the inset of Fig. 6 the τ/σ ratio vs temperature is shown. One can see that at low and high temperatures τ/σ is close to unity, proving the Poissonian statistics. At intermediate temperatures, τ/σ is significantly lower than unity, reaching the minimum value of 0.73 at 47 mK. This is evidence of the super-Poissonian distribution of photons, also known as photon bunching.

The time intervals between the events are presented as switching time distributions in Fig. 6 and fitted with an exponential distribution (dashed curves). This probability density for noise-induced escapes (or tunneling) across (through) the barrier should represent Poissonian distribution in the form $w(t) = \exp(-t/\tau)/\tau$ ⁵¹. One can see that the curve for 21 mK is fitted by the above exponential dependence without any fitting parameter for $\tau = 9.026$ s. The curve for 80 mK is also well-fitted by exponential dependence with $\tau = 7.214$ ms. In all cases, τ is taken directly from the experimental data as the mean time interval between the events. At the same time, at 47 mK, the switching time distribution is better fitted by the power dependence $t^{-\alpha}$ with $\alpha = 0.75$ (dotted curve) than by the exponential dependence with $\tau = 0.119$ s, at least for intermediate switching times. This is the evidence of quantum chaos⁴⁷ as natural statistics of thermal photons⁴⁵, see below. The change from Poissonian distribution at low temperatures to super-Poissonian at intermediate and back to Poissonian at high temperatures can be explained in the following way. At low temperatures, when the thermal photons in the cavity are very rare, the Poissonian statistics is the internal statistics of the detector as, e.g., for noise-induced escapes across a potential barrier⁵¹. With temperature increase, the contribution of thermal photons from a single 8.81 GHz mode starts to dominate, which, as argued in⁴⁵, should demonstrate the super-Poissonian statistics (see the mode contribution vs temperature in

Fig. 5b). With further increase of the temperature, the main 14 GHz mode starts to compete with the first one (their contributions become equal at 54 mK), which leads to Poissonization of the thermal photon statistics, according to⁴⁵. To our knowledge, this is the first direct observation of the super-Poissonian statistics of microwave thermal photons. The observation of super-Poissonian statistics of photons was proposed to be used as a signature of quantum chaos⁴⁷. Figure 7a shows the results of quantum chaos modeling⁴⁷, where the authors propose to use photon arrival histograms as a tool for observing quantum chaos. The authors compare the results of numerical simulations, and show that the statistics changes from Poissonian for regular dynamics to super-Poissonian in the case of the quantum chaos appearance. This is exactly the distribution observed in our experiment, shown in Fig. 7b, supporting the slogan: quantum chaos—non-linear linearity. Here, we should add, that while the cavity represents completely linear resonator, the total system is not linear, since the resonator is weakly coupled to the Josephson junction detector, which is a strongly nonlinear element.

Discussion

In this work we describe and operate a microwave single photon detector used to observe the clicking and the statistics of thermal photons emitted by a resonator at ultracryogenic temperatures. The Josephson junction-based sensor shows a sub-Hz dark count rate and high efficiency, combined with a reduced operation complexity compared to qubit-based designs^{23,24}. The SPD was used to observe single microwave photons emitted by a single-mode and a multi-mode thermal source, i. e. a copper cavity. Although widely accepted^{45,53,54}, an experimental demonstration of the super-Poissonian statistics of thermal microwave photons was, to our knowledge, missing. The measured photon rate is consistent with thermal emission from the microwave cavity modes, and closely follows the expected temperature dependence. The photon distribution displays a clear reduction of the mean-to-standard deviation ratio when the light is emitted mainly by one mode, which instead remains unitary for dark count and multi-mode emission. The dynamical range of the detector extends from its dark count rate to the kHz range and is currently limited by the acquisition electronics' speed. The detector dynamics was not further

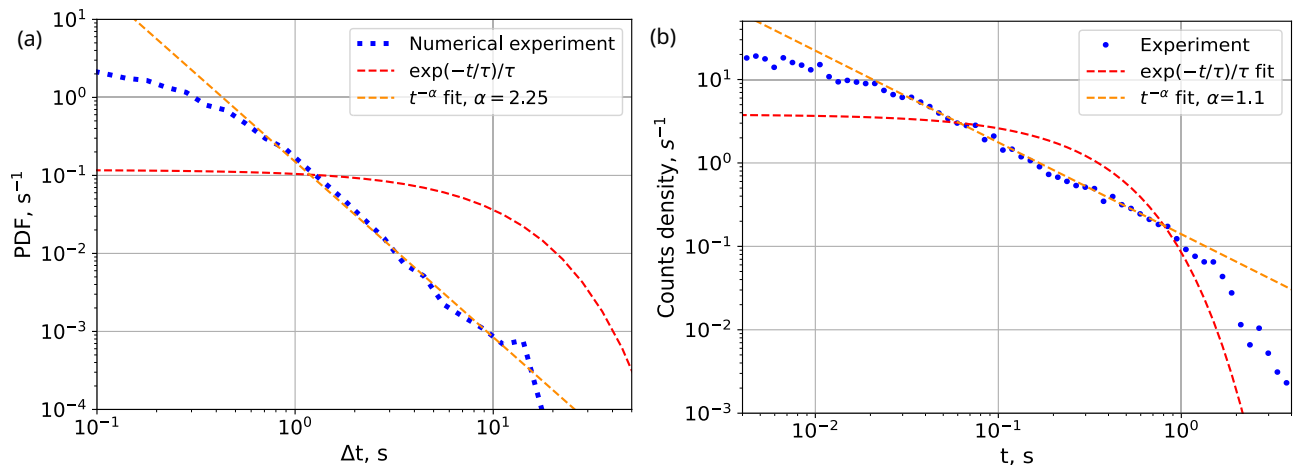


Fig. 7 | Comparison of Poissonian and super-Poissonian distributions. **a** Numerically computed distributions according to⁴⁷. **b** Measured switching time distribution (blue dots) of thermal photons from a cavity representing super-Poissonian distribution, fitted with exponent (red dashed curve) and $t^{-\alpha}$ dependence.

investigated and will be the subject of future works. The SPD efficiency can be better characterised with an on-demand microwave photon source^{55–58}, to disentangle it from other systematic uncertainties. Future efforts to improve the SPD aim mainly at improving its dark count rate. For instance, a junction with lower I_C could enter the phase diffusion regime, which is expected to increase its lifetime, and thereby reduce the dark count rate⁴⁴. Advancing the screening and filtering of the setup is also foreseen to improve the detector performance. In perspective, this work paves the way to a deeper examination of thermal light's quantum properties and to their use to study quantum chaos⁴⁷, ghost imaging^{59–61}, and more⁴⁵. The device itself finds numerous applications in the field of precision physics beyond the Standard Model, as for instance Axion searches^{34,35}. On the one hand, the performance requirements needed to drastically improve current Axion experiments are already met by the current device. On the other hand, these apparatus typically include strong magnetic field and long operation times, posing a challenge to the screening and long-term stability of the detector. Nevertheless, the implementation of single microwave photon detectors such as the one presented here fosters the emergence of next-generation beyond the Standard Model experiments^{42,62}.

Methods

Sample fabrication

The fabrication of a Josephson junction-based single photon detector requires a two-layer process. In the first Ti/Au/Pd multilayer, the contact pads, the antenna, and dc wires were fabricated at the nanofabrication facility of Chalmers university using laser-writer and lift-off technology. In the second layer, we patterned the superconductor-insulator-superconductor (SIS) tunnel junctions with the electron beam lithography. Thereafter, the SIS junction structures made of aluminum were deposited at NNSTU using a well-established shadow evaporation technique^{63,64} without breaking the vacuum. This technology is typically used for the fabrication of superconducting qubits that ensures long-time operation of the samples.

Shielding of the detector

The shielding of the setup from the environment is straightforward. The detector is readout with dc lines, filtered by the T-filters already described in the main text. Photons are emitted and measured inside the compact volume of the cavity and the detector holder without the need of any microwave cable, thereby ensuring a strong decoupling from the environment. External magnetic fields around the detector are screened by a two-layer cryoperm and superconducting screen.

Our experimental setup shows no sensitivity to either the Earth's magnetic field or nearby magnets.

Photon-assisted tunneling steps

The frequency response of the cavity at low temperatures was measured by using the photon-assisted tunneling steps of the SPD's IV curves⁶⁵, see Fig. 4. When the voltage at the junction is slightly lower than the doubled gap voltage, a single electron (quasiparticle) is able to tunnel from one side of the junction to another one. It becomes possible when $eV + hf > 2\Delta$ with V, f, Δ being voltage, emission frequency and superconducting energy gap, respectively. This effect appears in the IV curve of the junction as PAT step. The position of this step depends on the power of the incident signal while the voltage depends on its frequency.

Estimation of a single-photon-induced current pulse

Let us demonstrate that the Josephson junction works as a microwave single photon detector when its bias current I_b is slightly lower than the critical current I_C . As outlined in Fig. 1, the dynamics of a Josephson junction can be treated as the evolution of a phase particle in a tilted washboard potential. An absorbed photon causes a current pulse ΔI through the junction, overcoming the threshold, and thus leading to the appearance of measurable resistive state with a finite voltage of about 0.4 mV. In the Josephson circuit, the energy hf of the incoming photon is split between the energy of the supercurrent E_s stored in the tank circuit and the energy E_d dissipated in the subgap resistor R_{sp} , approaching R_N close to zero voltage, according to quasiparticle IV curve of a tunnel Josephson junction⁶⁶. Assuming the simple relation between E_s and the pulse amplitude ΔI ⁴², $E_s = L_{JJ}\Delta I^2/2$, and taking into account that in parallel RLC-resonant circuit $Q = R_N(C/L_{JJ})^{1/2}$, $E_s/E_d = Q/2\pi$, the current increase due to the photon can be estimated as $\Delta I = \sqrt{2hfL_{JJ}^{-1}(1 + 2\pi/Q)^{-1}}$, where the junction inductance L_{JJ} depends on the bias current I as $L_{JJ} = \hbar/(2e)(I_C^2 - I^2)^{-1/2}$. Using the above parameters, for $I_C = 170$ nA the single photon current pulse ΔI is estimated about 60 nA.

Data availability

The data that support the findings of this study are included into Supplementary materials. Source data are provided with this paper.

References

1. Glauber, R. J. Nobel lecture: One hundred years of light quanta. *Rev. Mod. Phys.* **78**, 1267–1278 (2006).

2. Amenomori, M. et al. First detection of photons with energy beyond 100 tev from an astrophysical source. *Phys. Rev. Lett.* **123**, 051101 (2019).
3. Natarajan, C. M., Tanner, M. G. & Hadfield, R. H. Superconducting nanowire single-photon detectors: physics and applications. *Superconduct. Sci. Technol.* **25**, 063001 (2012).
4. Walsh, E. D. et al. Josephson junction infrared single-photon detector. *Science* **372**, 409–412 (2021).
5. Kouwenhoven, K. et al. Resolving power of visible-to-near-infrared hybrid β - Ta/Nb - Ti - N kinetic inductance detectors. *Phys. Rev. Appl.* **19**, 034007 (2023).
6. Bettini, A. *Introduction to elementary particle physics; 1st ed.* <https://cds.cern.ch/record/1111396> (Cambridge Univ. Press, Cambridge, 2008).
7. Hadfield, R. H. Single-photon detectors for optical quantum information applications. *Nat. Photonics* **3**, 696–705 (2009).
8. Esmaeil Zadeh, I. et al. Superconducting nanowire single-photon detectors: A perspective on evolution, state-of-the-art, future developments, and applications. *Appl. Phys. Lett.* **118** (2021).
9. Khasminkaya, S. et al. Fully integrated quantum photonic circuit with an electrically driven light source. *Nat. Photonics* **10**, 727–732 (2016).
10. Irwin, K. D & Hilton, G. C. *Transition-Edge Sensors.* (Springer, Berlin: Heidelberg, Germany, 2005) 63–150.
11. Gleyzes, S. et al. Quantum jumps of light recording the birth and death of a photon in a cavity. *Nature* **446**, 297–300 (2007).
12. Astafiev, O. et al. Single-photon detector in the microwave range. *Appl. Phys. Lett.* **80**, 4250–4252 (2002).
13. Govenius, J., Lake, R. E., Tan, K. Y. & Möttönen, M. Detection of Zeptojoule Microwave Pulses Using Electrothermal Feedback in Proximity-Induced Josephson Junctions. *Phys. Rev. Lett.* **117**, 030802 (2016).
14. Lee, G.-H. et al. Graphene-based Josephson junction microwave bolometer. *Nature* **586**, 42–46 (2020).
15. Kokkoniemi, R. et al. Bolometer operating at the threshold for circuit quantum electrodynamics. *Nature* **586**, 47–51 (2020).
16. Blais, A., Grimsmo, A. L., Girvin, S. M. & Wallraff, A. Circuit quantum electrodynamics. *Rev. Mod. Phys.* **93**, 025005 (2021).
17. Royer, B., Grimsmo, A. L., Choquette-Poitevin, A. & Blais, A. Itinerant Microwave Photon Detector. *Phys. Rev. Lett.* **120**, 203602 (2018).
18. Grimsmo, A. L. et al. Quantum Metamaterial for Broadband Detection of Single Microwave Photons. *Phys. Rev. Appl.* **15**, 034074 (2021).
19. Johnson, B. R. et al. Quantum non-demolition detection of single microwave photons in a circuit. *Nat. Phys.* **6**, 663–667 (2010).
20. Inomata, K. et al. Single microwave-photon detector using an artificial Λ -type three-level system. *Nat. Commun.* **7**, 1–7 (2016).
21. Kono, S., Koshino, K., Tabuchi, Y., Noguchi, A. & Nakamura, Y. Quantum non-demolition detection of an itinerant microwave photon. *Nat. Phys.* **14**, 546–549 (2018).
22. Lescanne, R. et al. Irreversible Qubit-Photon Coupling for the Detection of Itinerant Microwave Photons. *Phys. Rev. X* **10**, 021038 (2020).
23. Albertinale, E. et al. Detecting spins by their fluorescence with a microwave photon counter. *Nature* **600**, 434–438 (2021).
24. Dixit, A. V. et al. Searching for Dark Matter with a Superconducting Qubit. *Phys. Rev. Lett.* **126**, 141302 (2021).
25. Balembos, L. et al. Cyclically operated microwave single-photon counter with sensitivity of 10^{-22} W/ $\sqrt{\text{Hz}}$. *Phys. Rev. Appl.* **21**, 014043 (2024).
26. Besse, J.-C. et al. Single-Shot Quantum Nondemolition Detection of Individual Itinerant Microwave Photons. *Phys. Rev. X* **8**, 021003 (2018).
27. Sikivie, P. Invisible axion search methods. *Rev. Mod. Phys.* **93**, 015004 (2021).
28. Irastorza, I. G. & Redondo, J. New experimental approaches in the search for axion-like particles. *Prog. Part. Nucl. Phys.* **102**, 89–159 (2018).
29. Sushkov, A. O. Quantum Science and the Search for Axion Dark Matter. *Phys. Rev. X Quantum* **4**, 020101 (2023).
30. Braine, T. et al. Extended search for the invisible axion with the axion dark matter experiment. *Phys. Rev. Lett.* **124**, 101303 (2020).
31. Kwon, O. et al. First Results from an Axion Haloscope at CAPP around 10.7 μeV . *Phys. Rev. Lett.* **126**, 191802 (2021).
32. Adair, C. M. et al. Search for dark matter axions with cast-capp. *Nat. Commun.* **13**, 6180 (2022).
33. Crescini, N. et al. Axion Search with a Quantum-Limited Ferromagnetic Haloscope. *Phys. Rev. Lett.* **124**, 171801 (2020).
34. Lamoreaux, S. K., van Bibber, K. A., Lehnert, K. W. & Carosi, G. Analysis of single-photon and linear amplifier detectors for microwave cavity dark matter axion searches. *Phys. Rev. D.* **88**, 035020 (2013).
35. Barbieri, R. et al. Searching for galactic axions through magnetized media: The QUAX proposal. *Phys. Dark Universe* **15**, 135–141 (2017).
36. Clerk, A. A., Devoret, M. H., Girvin, S. M., Marquardt, F. & Schoelkopf, R. J. Introduction to quantum noise, measurement, and amplification. *Rev. Mod. Phys.* **82**, 1155–1208 (2010).
37. Braggio, C. et al. Quantum-enhanced sensing of axion dark matter with a transmon-based single microwave photon counter (2024). 2403.02321.
38. Oelsner, G. et al. Underdamped Josephson junction as a switching current detector. *Appl. Phys. Lett.* **103**, 142605 (2013).
39. Oelsner, G. et al. Detection of Weak Microwave Fields with an Underdamped Josephson Junction. *Phys. Rev. Appl.* **7**, 014012 (2017).
40. Chen, Y.-F. et al. Microwave Photon Counter Based on Josephson Junctions. *Phys. Rev. Lett.* **107**, 217401 (2011).
41. Poudel, A., McDermott, R. & Vavilov, M. G. Quantum efficiency of a microwave photon detector based on a current-biased Josephson junction. *Phys. Rev. B* **86**, 174506 (2012).
42. Kuzmin, L. S. et al. Single Photon Counter Based on a Josephson Junction at 14 GHz for Searching Galactic Axions. *IEEE Trans. Appl. Superconduct.* **28**, 2400505 (2018).
43. Revin, L. S. et al. Microwave photon detection by an Al Josephson junction. *Beilstein J. Nanotechnol.* **11**, 960–965 (2020).
44. Pankratov, A. L. et al. Towards a microwave single-photon counter for searching axions. *npj Quantum Inf.* **8**, 1–7 (2022).
45. Fox, M. *Quantum Optics: An Introduction*, **15** of *Oxford Master Series in Physics* (Oxford University Press, 2006).
46. Kovalenko, A. et al. Emergence of super-poissonian light from indistinguishable single-photon emitters. *Optica* **10**, 456–463 (2023).
47. Yusipov, I. I., Vershinina, O. S., Denisov, S. V. & Ivanchenko, M. V. Photon waiting-time distributions: A keyhole into dissipative quantum chaos. *Chaos* **30**, ArticleSequenceNumber:023107 (2020).
48. Pankratov, A. L., Ladeynov, D. A., Revin, L. S., Gordeeva, A. V. & Ilichev, E. V. Quantum and phase diffusion crossovers in small Al Josephson junctions. *Chaos Solitons Fractals* **184**, 114990 (2024).
49. Martinis, J. M. & Grabert, H. Thermal enhancement of macroscopic quantum tunneling: Derivation from noise theory. *Phys. Rev. B* **38**, 2371–2379 (1988).
50. Golubev, D. S., Il'ichev, E. V. & Kuzmin, L. S. Single-Photon Detection with a Josephson Junction Coupled to a Resonator. *Phys. Rev. Appl.* **16**, 014025 (2021).
51. Malakhov, A. N. & Pankratov, A. L. *Evolution Times of Probability Distributions and Averages — Exact Solutions of the Kramers' Problem*, chap. 6, 357–438 (John Wiley & Sons, Ltd, Hoboken, NJ, USA, 2002).
52. Pozar, D. *Microwave Engineering, 4th Edition* <https://books.google.fr/books?id=JegbAAAQBAJ> (Wiley, 2011).

53. Morgan, B. L. & Mandel, L. Measurement of photon bunching in a thermal light beam. *Phys. Rev. Lett.* **16**, 1012–1015 (1966).
54. Boitier, F., Godard, A., Rosencher, E. & Fabre, C. Measuring photon bunching at ultrashort timescale by two-photon absorption in semiconductors. *Nat. Phys.* **5**, 267–270 (2009).
55. Bozyigit, D. et al. Antibunching of microwave-frequency photons observed in correlation measurements using linear detectors. *Nat. Phys.* **7**, 154–158 (2011).
56. Lang, C. et al. Observation of Resonant Photon Blockade at Microwave Frequencies Using Correlation Function Measurements. *Phys. Rev. Lett.* **106**, 243601 (2011).
57. Peng, Z. H., de Graaf, S. E., Tsai, J. S. & Astafiev, O. V. Tuneable on-demand single-photon source in the microwave range. *Nat. Commun.* **7**, 1–6 (2016).
58. Zhou, Y., Peng, Z., Horiuchi, Y., Astafiev, O. V. & Tsai, J. S. Tunable Microwave Single-Photon Source Based on Transmon Qubit with High Efficiency. *Phys. Rev. Appl.* **13**, 034007 (2020).
59. Gatti, A., Brambilla, E., Bache, M. & Lugiato, L. A. Ghost imaging with thermal light: Comparing entanglement and classical correlation. *Phys. Rev. Lett.* **93**, 093602 (2004).
60. Ou, L.-H. & Kuang, L.-M. Ghost imaging with third-order correlated thermal light. *J. Phys. B: At., Mol. Opt. Phys.* **40**, 1833 (2007).
61. Liu, Q., Chen, X.-H., Luo, K.-H., Wu, W. & Wu, L.-A. Role of multi-photon bunching in high-order ghost imaging with thermal light sources. *Phys. Rev. A* **79**, 053844 (2009).
62. Jaeckel, J. & Ringwald, A. The low-energy frontier of particle physics. *Annu. Rev. Nucl. Part. Sci.* **60**, 405–437 (2010).
63. Gordeeva, A. V. et al. Record electron self-cooling in cold-electron bolometers with a hybrid superconductor-ferromagnetic nanoabsorber and traps. *Sci. Rep.* **10**, 1–10 (2020).
64. Moskalev, D. O. et al. Optimization of shadow evaporation and oxidation for reproducible quantum Josephson junction circuits. *Sci. Rep.* **13**, 1–10 (2023).
65. Tien, P. K. & Gordon, J. P. Multiphoton Process Observed in the Interaction of Microwave Fields with the Tunneling between Superconductor Films. *Phys. Rev.* **129**, 647–651 (1963).
66. Barone, A. & Paternò, G. *Physics and applications of Josephson effect*. (John Wiley & Sons, New York, 1982).

Acknowledgements

The work is supported by the Russian Science Foundation (Project No. 19-79-10170). N.C. acknowledges the support from the Italian Institute of Nuclear Physics (INFN) within the QUAX experiment. The authors wish to thank G. Carugno for triggering the interest on photon detectors and for the multiple advice in the course of this work, A.A. Yablokov for writing an automated Python-based software, and I.V. Rakut' for sample holder fabrication. The numerical data shown in Fig. 7a to demonstrate a qualitative view of a super-Poissonian distribution as a hallmark of quantum chaos is a courtesy of Yusipov I.I. et al.⁴⁷.

Author contributions

The general idea of the work was suggested by L.S.K., N.C., A.V.G. and A.L.P. The sample fabrication was performed by A.V.G. and A.V.B. A.L.P. ran the experiment with support of A.V.G., A.V.C. and L.S.R. Data were analyzed by N.C., A.L.P., A.V.G. and A.V.C. A.L.P., A.V.G., L.S.R. and A.V.B. designed and assembled the experiment. The cavity was designed by N.C., and tested by N.C., A.L.P., A.V.G. and A.V.C. All authors, led by N.C. and A.L.P., contributed to manuscript with figures created by N.C., A.V.G. and A.V.C.

Competing interests

The authors declare no competing interests.

Additional information

Supplementary information The online version contains supplementary material available at <https://doi.org/10.1038/s41467-025-56040-4>.

Correspondence and requests for materials should be addressed to A. L. Pankratov or A. V. Gordeeva.

Peer review information *Nature Communications* thanks Steve Lamoreaux and Alex Opremcak for their contribution to the peer review of this work. A peer review file is available.

Reprints and permissions information is available at <http://www.nature.com/reprints>

Publisher's note Springer Nature remains neutral with regard to jurisdictional claims in published maps and institutional affiliations.

Open Access This article is licensed under a Creative Commons Attribution-NonCommercial-NoDerivatives 4.0 International License, which permits any non-commercial use, sharing, distribution and reproduction in any medium or format, as long as you give appropriate credit to the original author(s) and the source, provide a link to the Creative Commons licence, and indicate if you modified the licensed material. You do not have permission under this licence to share adapted material derived from this article or parts of it. The images or other third party material in this article are included in the article's Creative Commons licence, unless indicated otherwise in a credit line to the material. If material is not included in the article's Creative Commons licence and your intended use is not permitted by statutory regulation or exceeds the permitted use, you will need to obtain permission directly from the copyright holder. To view a copy of this licence, visit <http://creativecommons.org/licenses/by-nc-nd/4.0/>.

© The Author(s) 2025